Separation Science and Technology
Publication details, including instructions for authors and subscription information:
http://www.informaworld.com/smpp/title~content=t713708471

Novel Internally Staged Permeator Designs Using a Hollow Fiber Fabric

B. Liu[a]; X. Wu[a]; G. G. Lipscomb[a]; J. Jensvold[b]
[a] CHEMICAL & ENVIRONMENTAL ENGINEERING DEPARTMENT, UNIVERSITY OF TOLEDO, TOLEDO, OHIO, USA [b] MG GENERON, PITTSBURG, CALIFORNIA, USA

Online publication date: 19 June 2000

To cite this Article Liu, B. , Wu, X. , Lipscomb, G. G. and Jensvold, J.(2000) 'Novel Internally Staged Permeator Designs Using a Hollow Fiber Fabric', Separation Science and Technology, 35: 8, 1153 — 1177
To link to this Article: DOI: 10.1081/SS-100100217
URL: http://dx.doi.org/10.1081/SS-100100217

SEPARATION SCIENCE AND TECHNOLOGY, **35**(8), pp. 1153–1177, 2000

Novel Internally Staged Permeator Designs Using a Hollow Fiber Fabric

B. LIU, X. WU, and G. G. LIPSCOMB*
CHEMICAL & ENVIRONMENTAL ENGINEERING DEPARTMENT
UNIVERSITY OF TOLEDO
TOLEDO, OHIO 43606-3390, USA

J. JENSVOLD
MG GENERON
PITTSBURG, CALIFORNIA, USA

ABSTRACT

Five novel internally staged permeator (ISP) designs for membrane-based gas separations are described. Two permeate streams, a low-pressure and an intermediate-pressure permeate, and a high-pressure retenate stream are produced in an ISP. Three of the new designs utilize a woven fabric or alternating sheets of fibers to enable contacting patterns that are not possible with previous designs. All designs are compared for the production of an enriched oxygen permeate from air. Design and operational parameters were selected to maximize the recovery of the enriched oxygen product. Of the new designs, the best performer is the co-cross design. The best overall performer is the co-counter design. The co-cross design is able to recover 33% of the feed as a 42% oxygen permeate while the co-counter design is able to recover 35% of the feed in contrast to the 12% recovery provided by a single countercurrent stage. However, this increase in recovery comes at the expense of a significant increase in required membrane area: the co-cross design requires 20× more area than the countercurrent stage while the co-counter design requires 23× more area. All ISP designs are capable of producing higher permeate purities than achievable in a single countercurrent stage. The co-counter design can recover 12% of the feed as a 52% oxygen permeate while a single countercurrent stage is limited to purities less than 45%.

* To whom correspondence should be addressed. Telephone: (419) 530-8088. FAX: (419) 530-8086. E-mail: glenn.lipscomb@utoledo.edu

INTRODUCTION

Membrane-based gas separation processes are replacing other processes at an increasing rate (1). Their growth is fueled by the development of new materials with superior transport properties, new membrane formation processes, and new module designs. While the literature is replete with attempts to develop new materials with better membrane transport properties, less attention has been given to module design, and a significant portion of it is discussed only in the patent literature.

We consider here module designs that utilize membranes in hollow fiber form. The module contacts two different gas streams, on opposite sides of the membrane (internal and external to the fiber), without directly mixing them. The gas streams are at different pressures, which drives gas permeation across the membrane.

Gas permeation rates are directly proportional to partial pressure differences (1). The proportionality constant is the product of the membrane permeation area and permeance (the intrinsic permeability divided by the effective diffusion distance) for the gas-membrane pair. In a binary gas mixture, one species will possess a higher permeance (the fast gas) and permeation will concentrate this component in the low-pressure gas phase. The ratio of the fast to slow gas permeances, the permselectivity, indicates how effectively a membrane can separate a mixture.

Module designs have relied heavily on heat exchanger designs for controlling the contacting of internal flows. Conventional designs rely on three primary contacting patterns for the low-pressure permeate and high-pressure retentate (2). In co-current flow the permeate and retentate streams flow parallel to one another. In countercurrent flow the permeate and retentate streams flow in opposite directions. In crossflow the permeate and retentate flow in mutually perpendicular directions.

The performance of the three conventional module designs is well known (3). The best performance is obtained from the countercurrent design. Performance models and their solutions are well documented in the literature for binary (4–9) and multicomponent separations (10–13).

To improve the performance of these basic designs, one can either introduce a portion of one of the product streams back into the same module or send it to another module. Permeate recycle schemes (14, 15) are an example of the former while module cascades (16–18), including the continuous membrane column (19, 20), are examples of the latter. Several ingenious designs permit cascading within a single fiber bundle through the use of internal baffles or other design features (21–24). In comparison to external staging, internally staged designs require less plumbing and fewer module housings. However, the cost of manufacture is higher due to increased complexity.

Ohno and collaborators (25) proposed a dramatically different form of internal staging. In their designs, membranes made from two *different* materials are combined to permit contacting of the feed with both membranes simultaneously. Two low-pressure permeate streams are produced in addition to the retentate. This design is attractive if two membranes exist such that one possesses a permselectivity greater than 1 and the other a permselectivity less than 1: the faster permeating species is different for the two materials. Unfortunately, materials with the requisite transport properties are available only for a limited number of separations.

A significant modification of the two-membrane internally staged design is the internally staged permeator (ISP). An ISP uses the same membrane material for the two stages and produces an intermediate-pressure permeate stream that contacts both stages. As originally proposed by Sidhoum et al. (26), the ISP consists of a bundle of hollow fibers divided into two separate fiber groups. The two groups are uniformly mixed within the bundle but are separated at the ends and potted in separate tubesheets as illustrated in Fig. 1(a). This allows one to independently control the flow and pressure within each fiber group. In operation, the high pressure feed to one set of fibers (the first stage) produces a permeate at an intermediate pressure. This permeate simultaneously contacts the second fiber group (the second stage) to produce a lower pressure permeate. The concentration of the faster permeating species in the low pressure permeate can be greatly enriched over that achievable in a conventional design. This enrichment comes at the cost of lower membrane productivity.

Five ISP flow configurations have been investigated: 1) well-mixed (26–28), 2) co-co (26–28), 3) counter-counter (26–28), 4) co-counter (29), and 5) counter-co (29). Except for the well-mixed design, the first identifier used to describe a design refers to how the retentate and intermediate-pressure permeate are contacted while the second identifier refers to how the intermediate and low-pressure permeate are contacted. This is illustrated in Fig. 2. For example, in the co-co design the retentate and intermediate-pressure permeate contact co-currently and the intermediate and low-pressure permeates contact co-currently. Chen et al. (29) concluded that the co-counter design is the best performer of these designs. ISP designs also can provide superior performance to a two-stage cascade (26, 30).

ISP performance depends strongly on the intermediate-pressure permeate to retentate pressure ratio. Typically, the overall pressure ratio (low-pressure permeate to retentate pressure ratio) is specified, but how this pressure driving force is split between the two stages is not. Li et al. (27) show that an optimum value exists to maximize enrichment of the low-pressure permeate. They also demonstrate that an optimum value for the ratio of permeation area for the two stages exists.

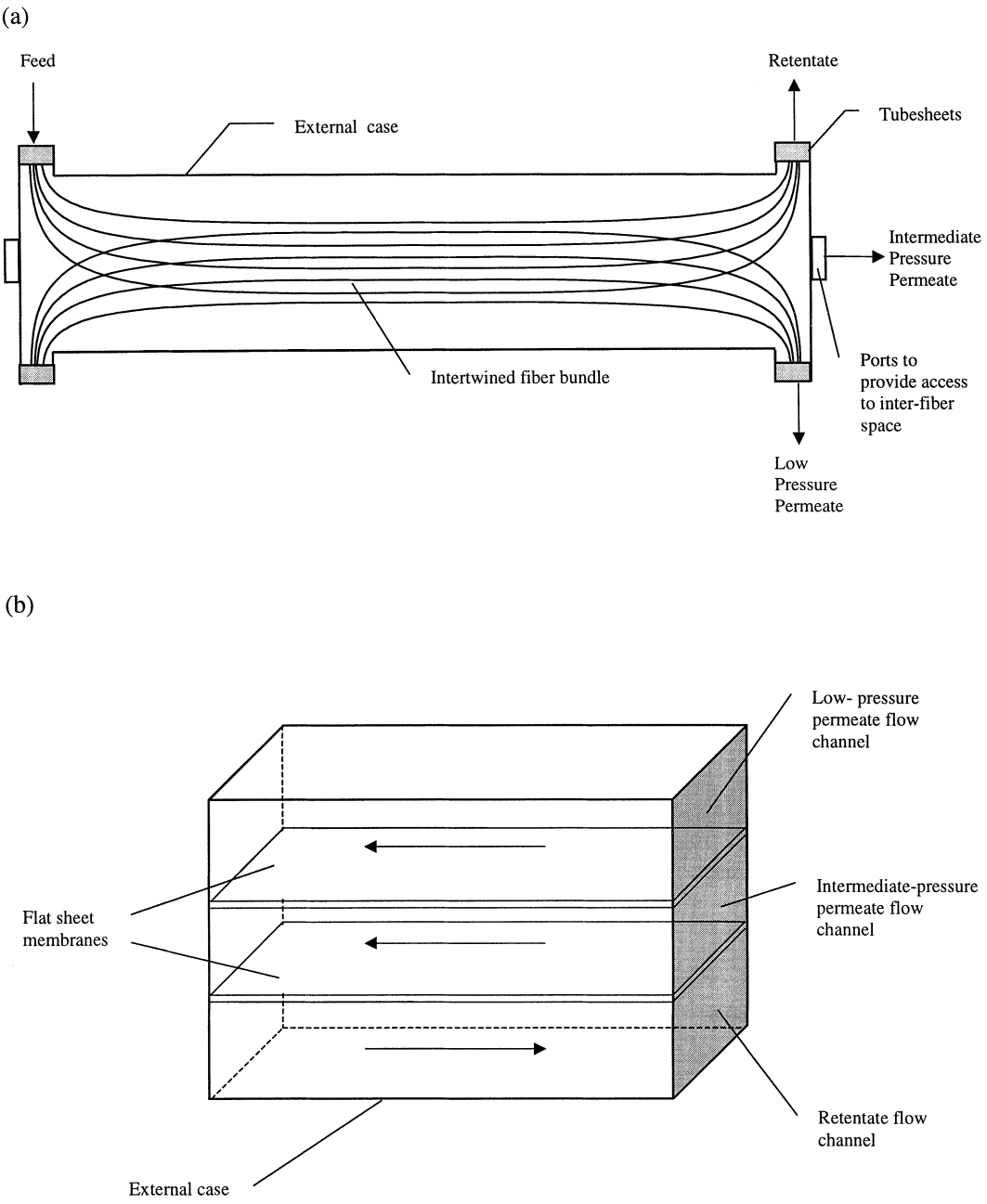

FIG. 1 Different realizations of ISP designs: (a) design based on a bundle of parallel hollow fiber membranes (the indicated flows correspond to the co-co design), (b) design based on flat sheet membranes (the indicated flows correspond to the counter-co design), (c) design based on concentric hollow fiber membranes (the indicated flows correspond to the co-counter design), and (d) design based on a hollow fiber membrane fabric or alternating sheets of parallel hollow fiber membranes (the indicated flows correspond to the cross-cross-cross design).

(c)

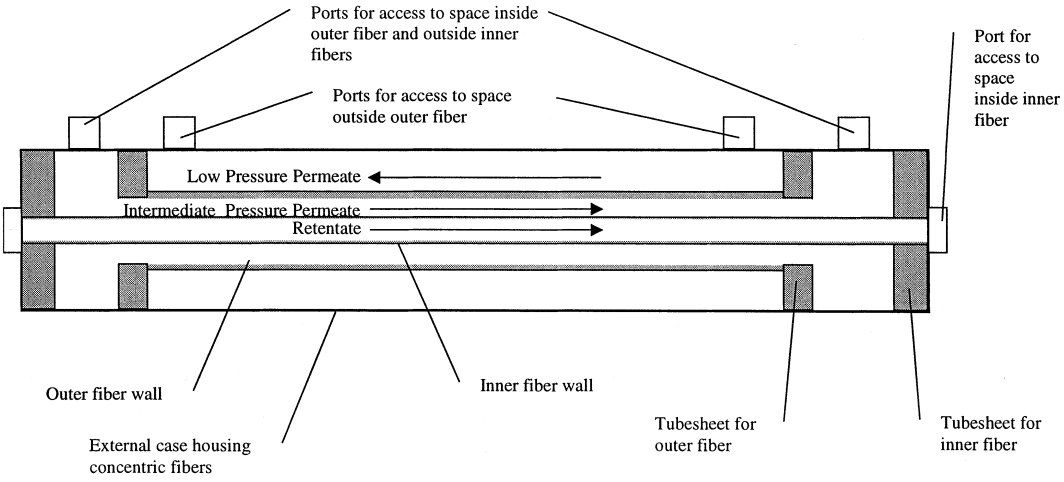

(d)

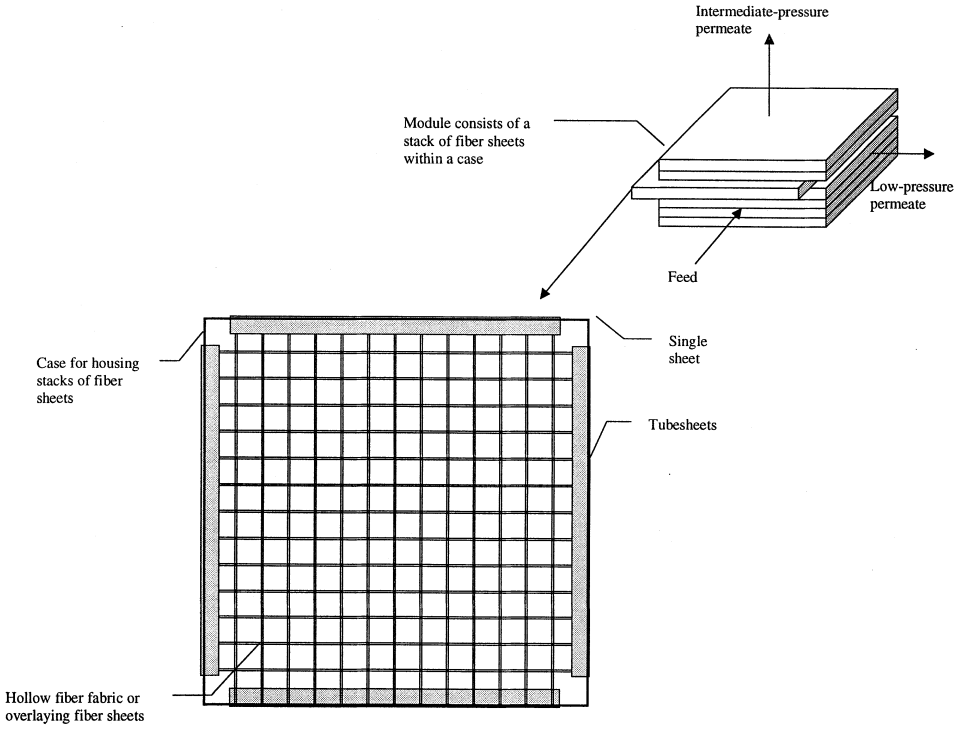

FIG. 1 Continued.

Although we will only consider hollow fiber membrane modules here, one can manufacture ISPs from flat sheet membranes (28) or concentric, annular hollow fiber membranes (31) as illustrated in Figs. 1(b) and 1(c), respectively. Additionally, one can include more than two stages in the design (32), but the

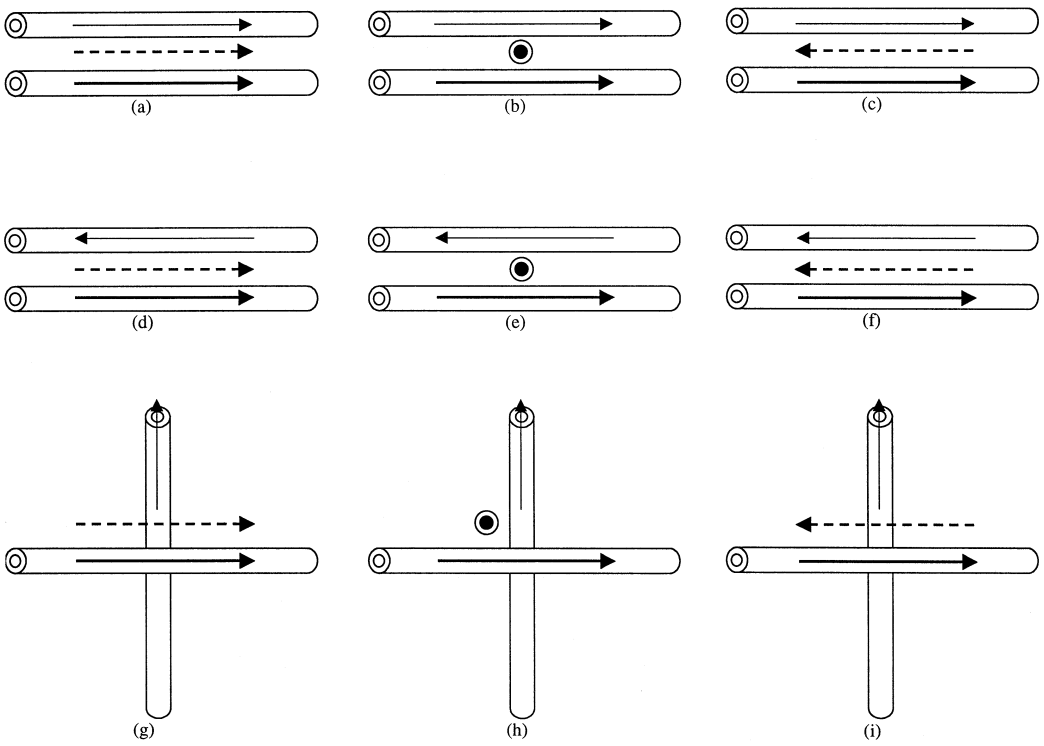

FIG. 2 Different ISP flow configurations. The thick solid arrow indicates the retentate flow direction which is always left to right. The thick dashed arrow indicates the intermediate-pressure permeate flow direction; a circle with a black dot inside indicates the intermediate-pressure permeate flows out of the plane of the paper. The thin solid arrow indicates the low-pressure permeate flow direction. The different configurations are: (a) co-co, (b) cross-cross-co, (c) counter-counter, (d) co-counter, (e) cross-cross-counter, (f) counter-co, (g) co-cross, (h) cross-cross-cross, (i) counter-cross.

inclusion of more stages appears to result in only modest performance improvements.

Here we examine a novel ISP design that uses hollow fiber fabrics, or fiber sheets, to generate the following contacting patterns: 1) cross-cross-cross, 2) co-cross, 3) counter-cross. Note that the third identifier refers to the contacting of the retentate and low-pressure permeate. It is required to distinguish the above from two additional flow patterns described later. Figure 1(d) illustrates the proposed module design while Fig. 2 illustrates the contacting patterns. One cannot generate cross-cross-cross contacting using parallel fiber bundles, flat sheet membranes, or concentric, annular hollow fibers. However, one could generate the other two configurations in a flat sheet module. We also consider two configurations that have not been considered before: 1) cross-cross-co and 2) cross-cross-counter. These flow patterns are illustrated in Fig. 2 as well. One can produce either contacting pattern in a parallel fiber bundle

MARCEL DEKKER, INC.
270 Madison Avenue, New York, New York 10016

or a flat sheet module. The performance of each design, except for the well mixed case, is evaluated for the production of an enriched oxygen stream from air. Module design and operation parameters are optimized to maximize the recovery of the enriched oxygen permeate. The results permit a detailed comparison of the designs.

ANALYSIS

To evaluate module performance, we make the following assumptions:

1. Constant pressure within each flow channel
2. Negligible concentration polarization
3. Negligible axial diffusion
4. Constant membrane transport properties
5. Isothermal operation
6. Binary gas mixtures

One can readily relax these assumptions as discussed in the literature (3), but models based on them appear to capture the essential physics of module operation and allow a self-consistent evaluation of different designs. Moreover, previous work (28, 29) indicates these assumptions lead to good agreement between theoretical calculations of ISP performance and experimental data. Note that the assumption of constant membrane transport properties does not imply constant mass transfer rates. Although one expects transport properties to be nearly constant for permanent gases such as oxygen and nitrogen (33), mass transfer rates which are given by the product of permeance and partial pressure difference change dramatically within the module.

The control volumes used to develop mass balances for the new designs are shown in Fig. 3. As for the previously described designs, the compositions of all streams change only in the retentate flow direction, the z direction. This conclusion is most difficult to visualize for the cross-cross-cross design, but permeate compositions will not vary in the x–y plane normal to the z direction if all fibers are identical. This is similar to a conventional crossflow module except that now there are two permeate streams which flow normal to the retentate flow *and* normal to each other.

Given the above assumptions, the dimensionless fast gas (i.e., more permeable component) permeation rate from the high-pressure retentate to the intermediate-pressure permeate, J^{A}_{HI}, is given by

$$J^{A}_{HI} = \alpha N_h (x - \gamma_{IH} y_I) \tag{1}$$

where "A" denotes the fast gas, α is the permselectivity, x is the fast gas mole fraction in the retentate, y_I is the fast gas mole fraction in the intermediate pressure permeate, and γ_{IH} is the ratio of the intermediate permeate to reten-

MARCEL DEKKER, INC.
270 Madison Avenue, New York, New York 10016

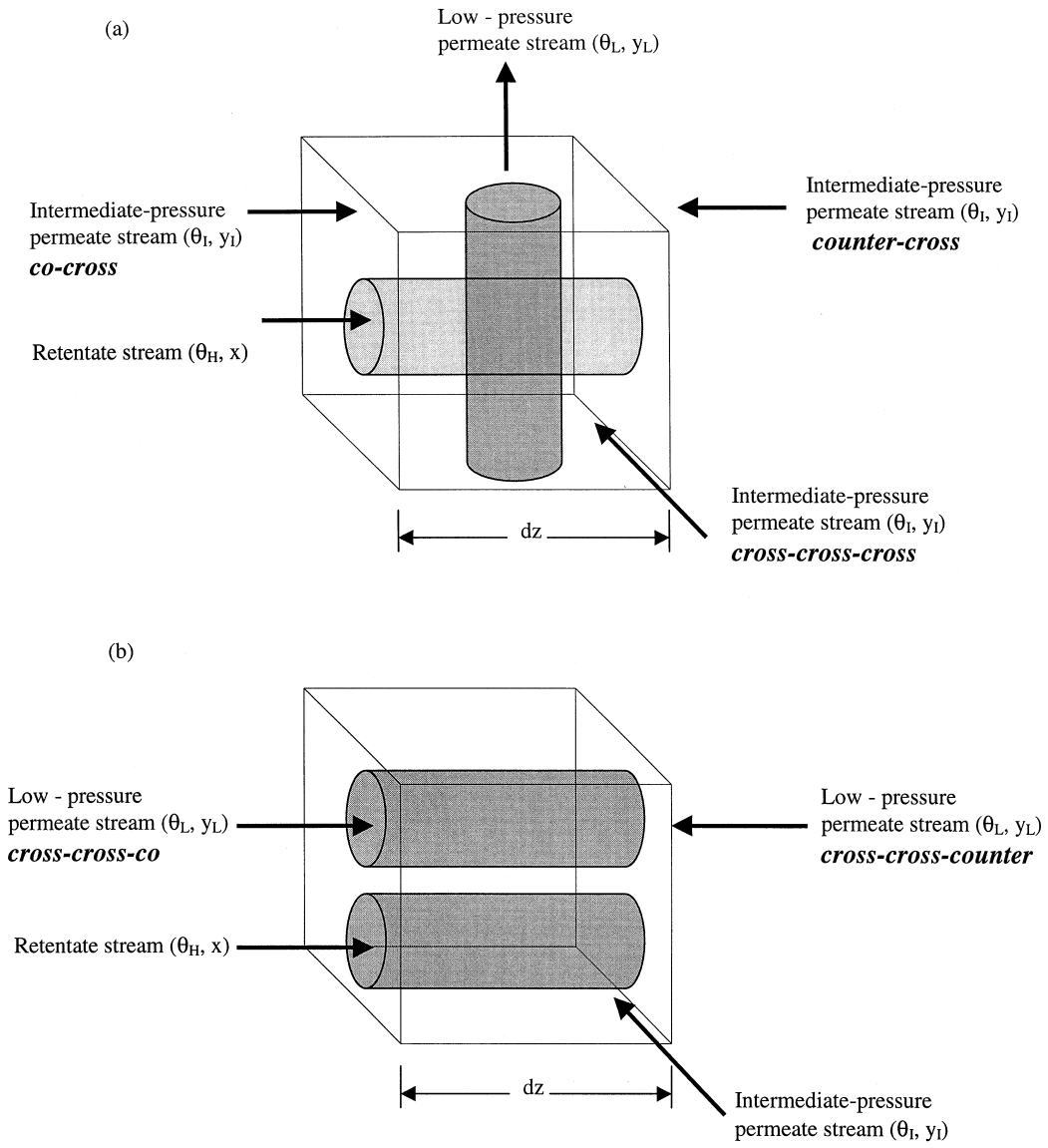

FIG. 3 Control volume used to develop mass balances for the new ISP designs: (a) control volume for designs utilizing a woven fiber fabric and (b) control volume for designs using parallel fibers. Arrows indicate flow directions.

tate pressure. Note that the subscript "H" refers to the retentate or high pressure stream and the subscript "I" refers to the intermediate-pressure permeate. N_h is a dimensionless mass transfer coefficient or membrane area defined as

$$N_h = A_{HI}\,(P/l)p_H/F \tag{2}$$

where A_{HI} is the total area available for permeation from the retentate to the intermediate-pressure permeate, P is the intrinsic slow gas permeability for

MARCEL DEKKER, INC.
270 Madison Avenue, New York, New York 10016

the membrane, l is the effective membrane thickness, p_H is the retentate pressure, and F is the total feed rate. One may also view N_h as a dimensionless inverse flow rate; increasing values of N_h correspond to decreasing flow rates if all other variables in Eq. (2) are held constant. The dimensionless slow gas permeation rate, J^B_{HI}, is given by

$$J^B_{HI} = N_h((1 - x) - \gamma_{IH}(1 - y_I)) \tag{3}$$

where "B" denotes the slow gas. The dimensionless fast gas permeation rate from the intermediate pressure permeate to the low pressure permeate is given by

$$J^A_{IL} = \alpha N_h \gamma_{IH} A_r (y_I - \gamma_{LI} y_L) \tag{4}$$

where A_r is the ratio of the area available for intermediate-to-low pressure permeation to the area available for high-to-intermediate pressure permeation, γ_{LI} is the ratio of low to intermediate permeate pressures, and y_L is the fast gas mole fraction in the low-pressure permeate. Likewise, the slow gas permeation rate is given by

$$J^B_{IL} = N_h \gamma_{IH} A_r ((1 - y_I) - \gamma_{LI}(1 - y_L)) \tag{5}$$

Note that the subscript "L" refers to the low-pressure permeate.

The literature documents the equations and solution procedures for the conventional countercurrent module and previously disclosed ISP designs. Model equations and their solutions for only the new designs will be discussed here. For the co-counter and counter-counter ISP designs, though, we found that solution algorithms using the finite difference approximation to represent derivatives converged more readily than algorithms using numerical integration with shooting (35); the shooting algorithm is described later for the counter-cross design.

For the *cross-cross-cross* ISP design, mass balances on the retentate stream (see Fig. 3a) require

$$\frac{d(x\theta_H)}{dz} = -J^A_{HI} \tag{6}$$

$$\frac{d((1 - x)\theta_H)}{dz} = -J^B_{HI} \tag{7}$$

for the fast and slow gases, respectively, where θ_H is the ratio of the retentate flow to the feed flow and z is the dimensionless flow path length. Mass balances on the intermediate- and low-pressure permeate streams reduce to the following simultaneous algebraic equations for the two permeate mole fractions:

$$y_I = \frac{J^A_{HI} - J^A_{IL}}{(J^A_{HI} - J^A_{IL}) + (J^B_{HI} - J^B_{IL})} \tag{8}$$

$$y_L = \frac{J_{IL}^A}{J_{IL}^A + J_{IL}^B} \tag{9}$$

To evaluate module performance, one must integrate Eqs. (6) and (7) from the feed location, $z = 0$, to the retentate exit, $z = 1$. All integrations were performed using the variable step, combined fourth-fifth order Runge–Kutta integration algorithm implemented in MATLAB as the function ODE45 (34). Numerical error was controlled to yield solutions accurate to three significant figures. At $z = 0$, θ_H equals unity while x equals the feed fast gas mole fraction: $x_f = 0.21$ for an air feed. Note that for a given x, one can solve Eqs. (8) and (9) for y_I and y_L using a Newton–Raphson iterative algorithm (35) and substitute the values into Eqs. (6) and (7).

For the *co-cross* ISP design, mass balances on the intermediate-pressure permeate stream (see Fig. 3a) yield

$$\frac{d(y_I\theta_I)}{dz} = J_{HI}^A - J_{IL}^A \tag{10}$$

$$\frac{d((1 - y_I)\theta_I)}{dz} = J_{HI}^B - J_{IL}^B \tag{11}$$

for the fast and slow gases, respectively, where θ_I is the ratio of the intermediate-pressure permeate flow to the feed flow. One must integrate Eqs. (6)–(7) and (10)–(11) to evaluate module performance. At $z = 0$, $\theta_H = 1$, $x = x_f$, and $\theta_I = 0$, y_I is given by the solution to Eq. (8). Note that for a given x and y_I, one can solve Eq. (9) for y_L and substitute the value into Eqs. (6)–(7) and (10)–(11).

For the *counter-cross* ISP design (see Fig. 3a), the intermediate-pressure mass balances are given by Eqs. (10) and (11) upon negating the left-hand side of each equation. Furthermore, the boundary conditions for the intermediate-pressure permeate now apply at $z = 1$ instead of $z = 0$. A shooting method is used to solve this split boundary value problem in which we guess values for x and θ_H at $z = 1$ and integrate backwards to $z = 0$. The guessed values are accepted if the calculated values for x and θ_H at $z = 0$ are sufficiently close to x_f and 1, respectively. Otherwise an improved guess is generated using an approximate Newton–Raphson procedure.

For the *cross-cross-co* ISP design, mass balances on the low-pressure permeate stream (see Fig. 3b) yield

$$\frac{d(y_L\theta_L)}{dz} = J_{IL}^A \tag{12}$$

$$\frac{d((1 - y_L)\theta_L)}{dz} = J_{IL}^B \tag{13}$$

for the fast and slow gases, respectively, where θ_L is the ratio of the low-pressure permeate flow to the feed flow. One must integrate Eqs. (6)–(7) and

(12)–(13) to evaluate module performance. At $z = 0$, $\theta_H = 1$, $x = x_f$, and $\theta_L = 0$, y_L is given by the solution to Eq. (9). Note that for a given x and y_L, one can solve Eq. (8) for y_I and substitute the value into Eqs. (6)–(7) and (12)–(13).

For the *cross-cross-counter* ISP design (see Fig. 3b), the low-pressure mass balances are given by Eqs. (12) and (13) upon negating the left-hand side of each equation. Furthermore, the boundary conditions for the low-pressure permeate now apply at $z = 1$ instead of $z = 0$. A shooting method similar to that described for the counter-cross ISP design is used to solve this split boundary value problem.

To evaluate the appropriateness of the constant pressure assumption, we will use the Hagen–Poiseuille law to calculate lumen pressure drops (3). Assuming ideal gas behavior, changes in lumen pressure are given by

$$d\Pi_i^2/dz = -N_p\theta_i \tag{14}$$

where Π is the dimensionless pressure (ratio of lumen pressure to feed pressure), the subscript i represents either the retentate (H) or low pressure permeate (L), and the dimensionless group N_p is given by

$$N_p = \frac{256\mu RTZF}{\pi ID^4 p_F^2} \tag{15}$$

where μ is the gas viscosity, R is the ideal gas constant, T is the temperature, Z is the active fiber length, ID is the fiber inner diameter, and p_F is the feed pressure. The appropriate boundary conditions for Eq. (14) are, at $z = 0$, $\Pi_H = 1$ for the retentate fibers and, at the low-pressure permeate outlet, $\Pi_L = p_L/p_F$ for the low-pressure permeate fibers where p_L is the outlet pressure for the low-pressure permeate.

For the performance calculations described here, we fixed α and the overall pressure ratio γ_{LH} (low pressure/high pressure) at 3.16 and 1/26, respectively. These values are identical to those used in a prior ISP study by Li et al. (27), and we were able to reproduce the results they reported. Since we will determine module performance over a range of product purities by varying the flow rate or N_h, two additional variables are freely adjustable: A_r and γ_{IH}. Note that $\gamma_{LI} = \gamma_{LH}/\gamma_{IH}$.

Ideally, one would choose values for A_r and γ_{IH} that optimize ISP performance. For the production of an enriched permeate, performance is characterized by: 1) the ratio of the product to the feed flow, the permeate recovery θ_L; and 2) the dimensionless area, N_h. Based on cost considerations, one would like to maximize θ_L *and* minimize N_h; increasing θ_L reduces gas compression costs while reducing N_h reduces membrane costs. If values for membrane and compression costs were known, one could minimize the cost of manufacture per unit volume of product to determine optimum values for A_r and γ_{IH}. Unfortunately, these costs, especially membrane costs, are difficult to estimate for the new ISP designs, which makes an economic optimization problematic.

An alternative is to optimize performance based on one of the performance criteria only. Here we seek values for A_r and γ_{IH} that maximize recovery, θ_L, only for a given product purity. Prior work suggests that ISP designs will be most attractive when membrane costs are small relative to compression costs, and maximizing recovery corresponds to minimizing compression costs. Moreover, a comparison of the various ISP designs in this limit provides a quantitative ranking of their performance capabilities which is the goal of the work presented here. The alternative of minimizing the required area for a given product purity possesses a trivial solution: for vanishingly small values of N_h the permeate composition takes on its maximum value, and one could mix this stream with a portion of the feed to produce any composition in-between. The procedures described next for performing the optimization could be used, however, to minimize the cost of manufacture if cost information was known.

To maximize θ_L, or equivalently minimize $1/\theta_L$, we use the Nelder–Mead simplex search algorithm implemented in MATLAB as the function FMINS (34). The search algorithm starts from an initial guess for A_r and γ_{IH} to find values that minimize $1/\theta_L$. Unfortunately, one cannot guarantee that a value returned by the algorithm corresponds to a global minimum. It may be a local minimum instead. This problem cannot be avoided because an optimization algorithm to find global extrema in finite time does not exist (35).

To assess if other local minima exist, we ran the search algorithm starting from different initial guesses and systematically searched the feasible parameter space for A_r and γ_{IH} by determining performance on a fine grid of points. Both approaches did not reveal the presence of any other minima.

RESULTS

The discussion of the results is divided into two sections: 1) parametric studies and 2) performance optimization. In the Parametric Studies section, the dependences of the low-pressure permeate composition (y_L) and recovery (θ_L) on the primary design variables (N_h, A_r, and γ_{IH}) are illustrated by changing one variable at a time. In the Performance Optimization section, the maximum value of θ_L achievable with each ISP design is presented as a function of y_L. The required dimensionless area is also given.

Parametric Studies

A parametric study of how N_h, A_r, and γ_{IH} influence performance is shown in Figs. 4–6. Figure 4 illustrates the effect of N_h on performance for the nine ISP designs for $A_r = 1.0$ and $\gamma_{IH} = 0.14$. Figure 4(a) indicates that the highest purity permeate, produced at zero recovery, is 0.58 for all of the ISP designs while that for the conventional countercurrent design is 0.44. In the limit

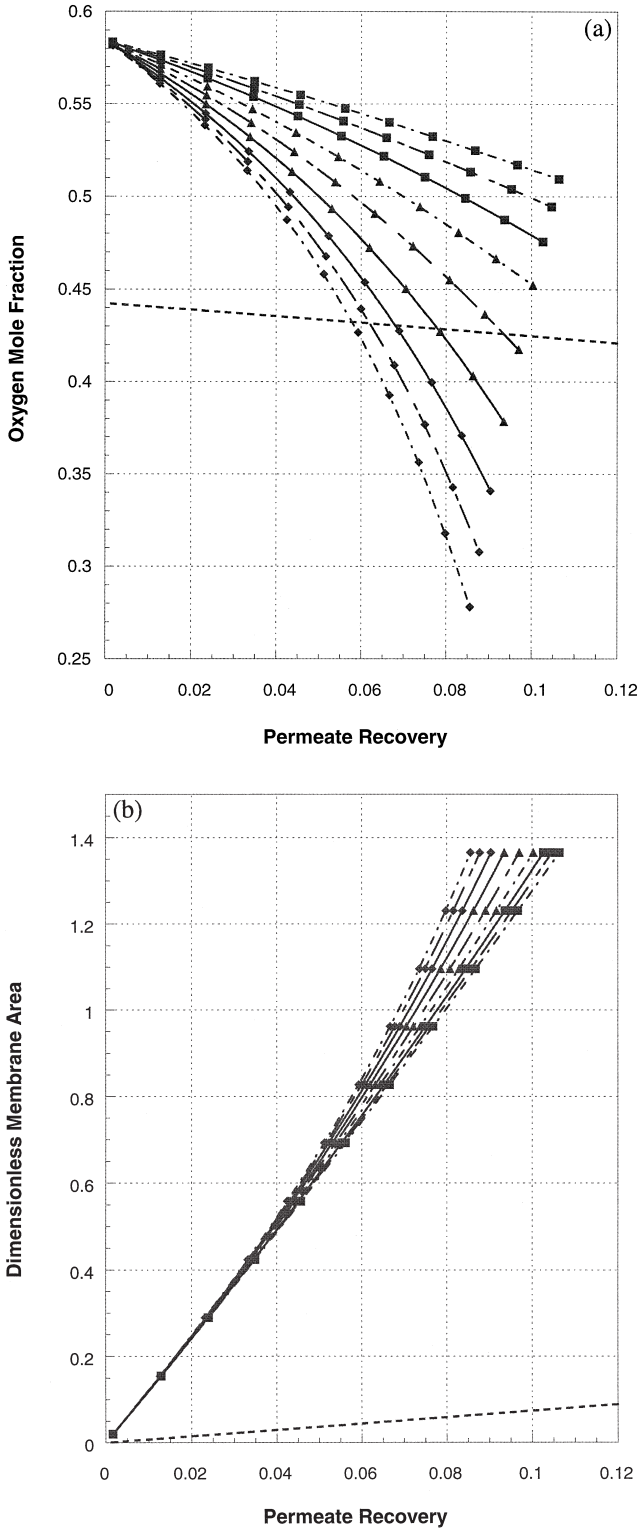

FIG. 4 The effect of N_h on ISP performance: (a) low-pressure permeate oxygen mole fraction and (b) dimensionless membrane area. The intermediate-pressure permeate and retentate contacting pattern is indicated by the symbols: co (■); counter (◆); cross-cross (▲). The low-pressure permeate and intermediate-pressure permeate contacting patterns are indicated by the line type: co (——); cross (— -); counter (–·). Results for a conventional countercurrent design are indicated by the dashed line.

MARCEL DEKKER, INC.
270 Madison Avenue, New York, New York 10016

of zero recovery, compositions do not vary along the length of the permeator and all ISP designs perform identically; the composition of the intermediate and low-pressure permeates are given by the solution to the cross-cross-cross design equations. Similarly, the three conventional designs perform like a cross flow module in the limit of zero permeate recovery.

As θ_L increases, y_L decreases as observed for the conventional countercurrent design. Although the rate of decrease is faster for the ISP designs, the purity for a given recovery is higher for all ISP designs at sufficiently low recoveries. This increase in y_L is a result of the two-stage permeation process. Permeation in a stepwise fashion from the high to the low pressure enhances the fast gas permeation rate relative to the slow gas permeation as observed previously (26). However, the absolute permeation rate decreases, which leads to an increase in the required permeation area. Figure 4(b) shows the total dimensionless area as a function of permeate recovery; the total dimensionless area is given by $(1 + A_r)N_h$. The required area increases much faster for the ISP designs than for the countercurrent design, and at the highest recoveries can be an order of magnitude larger.

Figure 4(a) indicates that as θ_L increases, y_L may become smaller than that achievable with a countercurrent stage. Why is ISP performance poorer than a countercurrent stage at higher recoveries? This behavior arises from the two-step permeation process. The permeate enrichment in ISP designs is strongly dependent on the pressure ratios γ_{IH} and γ_{LI}. If not selected properly, the ISP performs more poorly than a conventional countercurrent stage (see Fig. 6). The values used for γ_{IH} and γ_{LI} to produce Fig. 4(a) are not optimal. However, proper selection of these values leads to better performance as will be shown later (see Fig. 7).

The effect of increasing A_r for a fixed $N_h = 0.3$ and $\gamma_{IH} = 0.14$ is shown in Fig. 5. Values for A_r are not indicated, but A_r increases monotonically as one moves along the curve for any ISP design from left to right. Therefore, θ_L increases monotonically and y_L decreases monotonically with increasing A_r. Additionally, the performance of the ISP designs follows the order:

co-counter > **co**-cross > **co**-co >

cross-cross-counter > **cross**-cross-cross > **cross**-cross-co >

counter-co > **counter**-cross > **counter**-counter

We will find that the optimal performance of the ISP designs follows the same order. All of the designs with co-current contacting of the intermediate-pressure permeate and retentate perform better than the cross-contacting designs, which perform better than the countercurrent contacting designs. This indicates that contacting of the intermediate-pressure permeate and retentate has a greater impact on performance than contacting of the intermediate-pressure

and low-pressure permeate. Additionally, the order is the opposite of that observed for the conventional designs.

For the three designs with either co or cross contacting of the intermediate-pressure permeate and retentate, the design with countercurrent contacting of the low-pressure and intermediate-pressure permeate is the best performer followed by the cross design and then the co design. This order is the same as that observed for conventional designs. The designs with countercontacting of the intermediate-pressure permeate and retentate follow the opposite order.

The effect of γ_{IH} on performance is illustrated in Fig. 6. The value for γ_{IH} increases monotonically as one moves from left to right along each curve. The primary difference between Figs. 5 and 6 is the presence of a maximum y_L at an intermediate value of θ_L. This unique behavior of ISP designs differs from that of conventional designs in which purity increases monotonically as recovery decreases. This behavior also indicates that recovery is not a unique function of purity. The recovery may take on more than one value for a given purity. One would want to operate at the highest recovery possible, which can be an order of magnitude larger than the lowest recovery. For example, in-

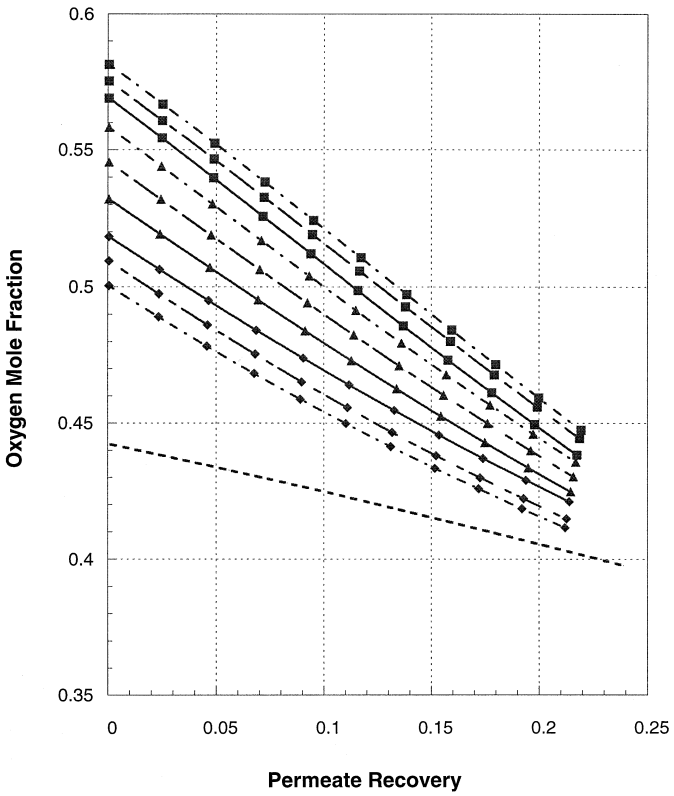

FIG. 5 The effect of A_r on ISP performance. See the Fig. 4 legend for the key.

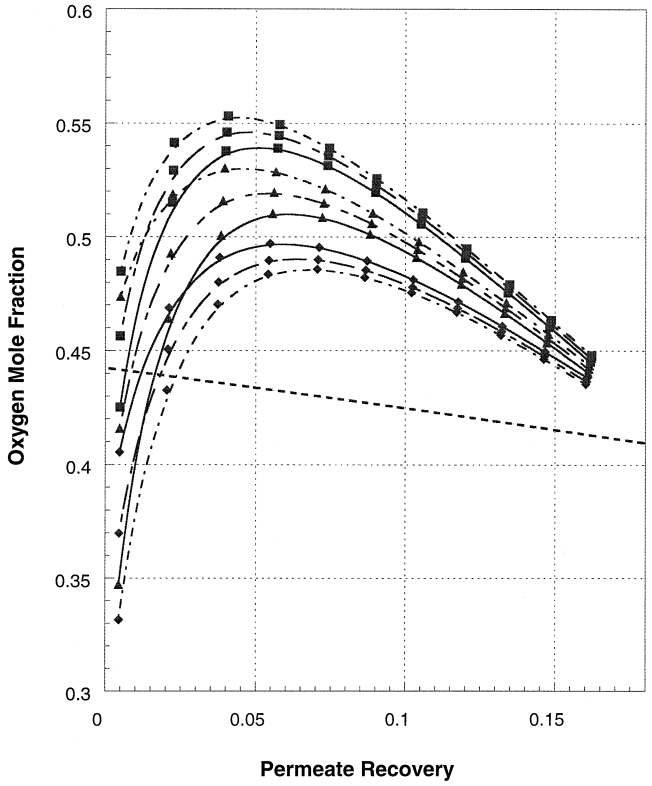

FIG. 6 The effect of γ_{IH} on ISP performance. See the Fig. 4 legend for the key.

creasing γ_{IH} from 0.05 to 0.34 increases the permeate recovery for the cocounter design from ~0.01 to ~0.13 at an oxygen mole fraction of ~0.48.

The maximum in y_L is due to the need for transport across two different stages: the high-to-intermediate pressure stage and the intermediate-to-low pressure stage. If the partial pressure driving force is too "low" for either stage, the enhancement of the fast gas in the permeate from that stage will be poor. The best overall enhancement occurs when the pressure ratio is equal for both stages, $\gamma_{IH} = \gamma_{LI}$, which is ~0.2 for the overall pressure ratio of 1/26 used here.

In Fig. 6, ISP performance follows the same order as observed previously. The maximum purity is higher than that achievable in a countercurrent stage at high recoveries but may be lower at low recoveries. The poorer performance at low recoveries is due to how recovery was varied to produce Fig. 6. Recovery was decreased by decreasing γ_{IH}. Since all other operating conditions were held constant, γ_{LI} was increased simultaneously to maintain a fixed overall pressure ratio (γ_{IH}*γ_{LI}). The increase in permeate purity achievable in an ISP occurs only when the pressure ratios γ_{IH} and γ_{LI} are comparable. Thus,

the enhancement is lost if the pressure ratios are not comparable, and this occurs at low recoveries in Fig. 6.

Performance Optimization

The results of the performance optimization are shown in Figs. 7 and 8. The performance of the ISP designs follows the same order as observed in Figs. 5 and 6. For a given y_L the co-counter design gives the highest recovery of all the designs. For an oxygen mole fraction of 0.42, the recovery is more than twice that achievable with a conventional countercurrent design. The relative increase in recovery becomes larger as purity increases. The co-cross design is the next best performer overall and is the best performer of the new designs proposed here. The recovery differences between the two are less than 5%.

The increase in recovery comes at the expense of increased area requirements as illustrated in Fig. 8. For an oxygen mole fraction of 0.42, the area required for the co-counter design is over *twenty times* that required for a countercurrent design. The area requirements fall in the same order as recovery.

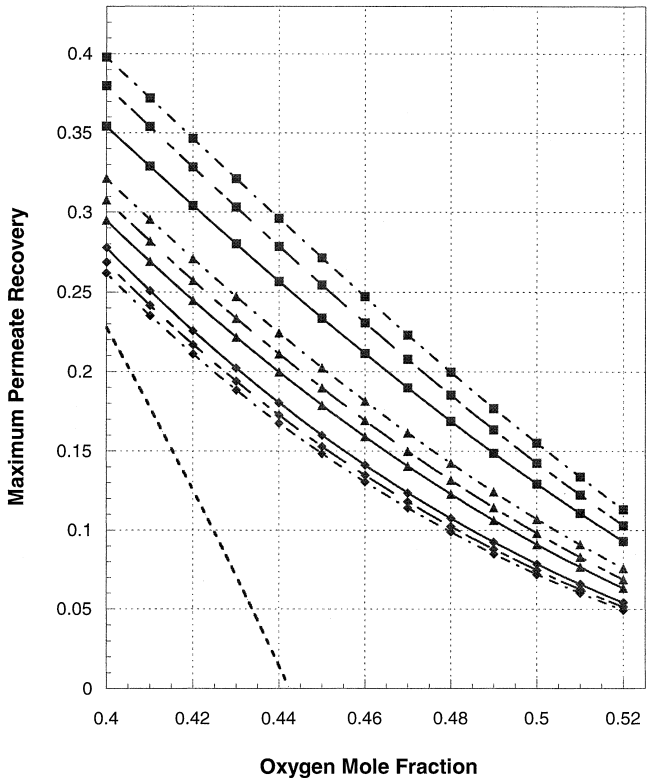

FIG. 7 Maximum ISP recovery for a given low-pressure permeate purity. Values for A_r and γ_{IH} were varied to maximize recovery. See the Fig. 4 legend for the key.

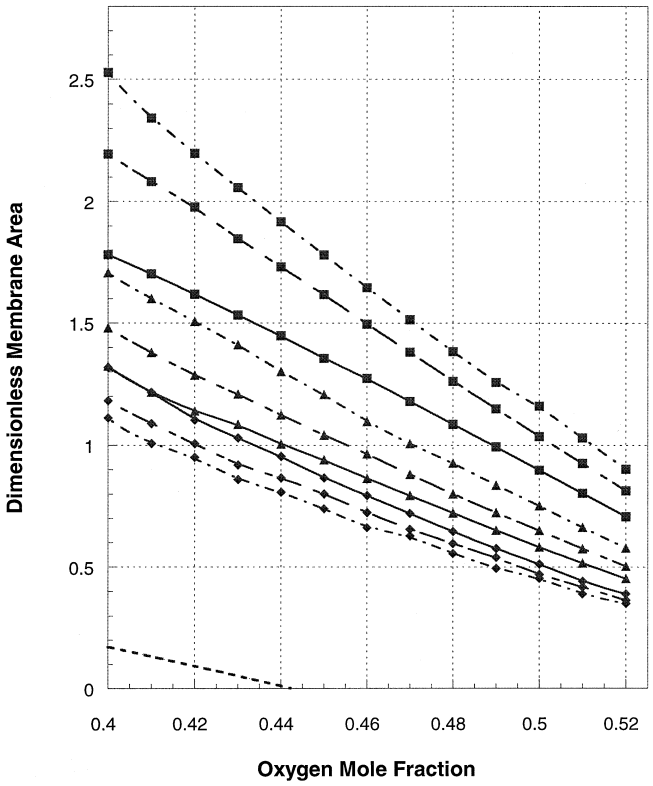

FIG. 8 Dimensionless membrane area required to maximize ISP recovery for a given low-pressure permeate purity. See the Fig. 4 legend for the key.

The different performance characteristics of the ISP designs provide an additional degree of freedom in module design. Because of economic considerations, one may opt for a design that offers lower recovery at a given purity because of lower area requirements. To make such a decision, though, one must know membrane and compression costs as discussed earlier.

The values of A_r and γ_{IH} that maximize recovery for a given purity change with purity and hence vary along each curve in Figs. 7 and 8. The range of values for the co-counter design is indicated in Table 1. Unfortunately, A_r cannot be varied easily. Economic considerations will dictate that one manufacture a limited number of modules with different area ratios.

To assess the effect of fixing A_r on performance, A_r was fixed at 1.5, a value in the middle of the optimum range for the co-counter design, and values of γ_{IH} that maximize recovery were determined using the optimization procedure described earlier. The results are shown in Figs. 9 and 10. The maximum permeate recovery achievable with fixed A_r is virtually identical to that with variable A_r. The required dimensionless area is slightly higher ($<15\%$) with fixed A_r at the highest permeate purities but lower at the lowest purities. The

TABLE 1
Range of Values for A_r and γ_{IH} Required to Maximize Permeate Recovery for Co-counter Design

Low-pressure permeate purity, y_L	A_r	γ_{IH}
0.40	2.0	0.21
0.42	1.9	0.21
0.44	1.7	0.21
0.46	1.5	0.21
0.48	1.3	0.21
0.50	1.2	0.20
0.52	1.0	0.20

changes are relatively small, though, and one could select an A_r value that minimizes the change in required area over the composition range of interest.

Figures 9 and 10 also contain results for fixing A_r at 1.5 *and* γ_{IH} at 0.21; both values fall in the middle of the optimum range. The reduction in recovery is

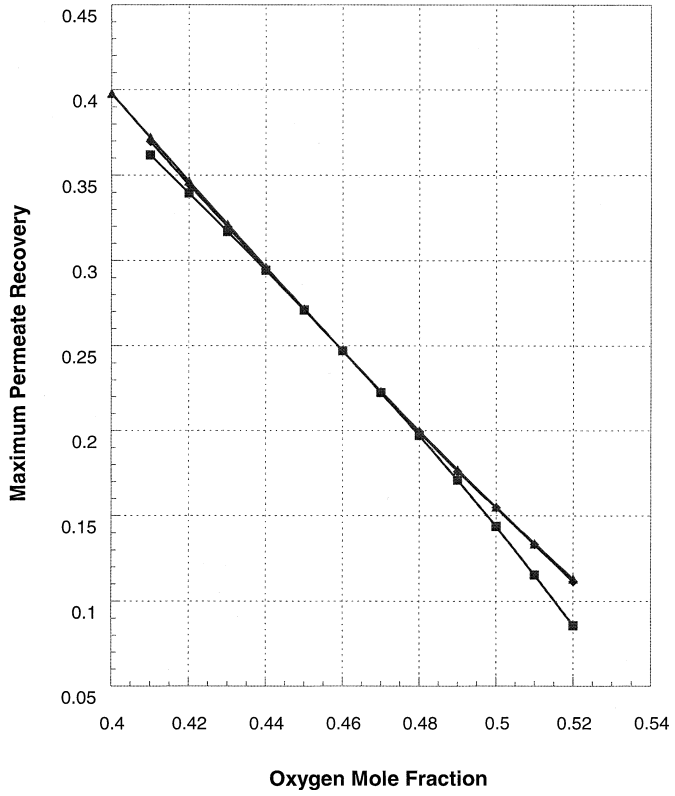

FIG. 9 Comparison of optimal co-counter ISP recovery (▲) to recovery with either fixed A_r (◆) or fixed A_r and γ_{IH} (■). Note that the results for the optimal design (▲) and fixed A_r design (◆) overlap.

MARCEL DEKKER, INC.
270 Madison Avenue, New York, New York 10016

more pronounced relative to the case in which only A_r was fixed. Additionally, the required dimensionless area is *lower*, relative to the maximum recovery result, at the highest permeate purities. This reduction, though, comes at the cost of reduced recovery. Such a tradeoff illustrates once again that one must be able to accurately assign membrane and compression costs to determine the economically optimum design.

The maximum permeate recovery changes little when the effects of lumen pressure drops are included. The values for maximum recovery and required area change by less than 1% for the co-co design when Eq. (14) is used to calculate pressure drop in the retentate and low-pressure permeate fibers. Table 2 contains values for the material parameters and module design variables used in the calculations; these values are representative of prior experimental work (27) and typical design values. Calculations for the other designs that account only for pressure drops in the feed fibers give similar results. Such observations are consistent with experimental data (29) that indicate pressure drops are small.

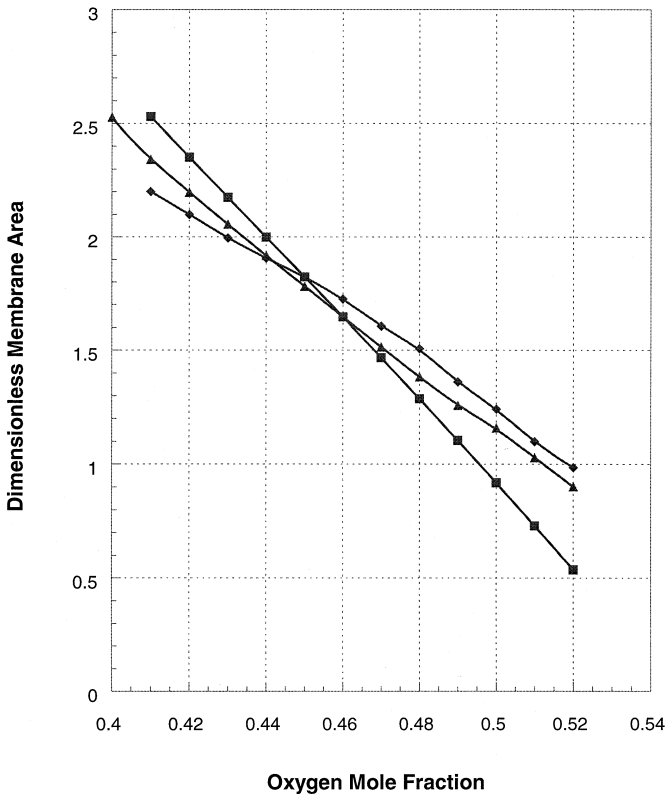

FIG. 10 Comparison of optimal co-counter ISP area requirements (▲) to area requirements with either fixed A_r (◆) or fixed A_r and γ_{IH} (■).

TABLE 2
Material Parameters and Operating Conditions
Used to Evaluate Lumen Pressure Drops

Parameter	Value
x_f	0.21
p_F	2600 kPa
p_L	100 kPa
(P/l) oxygen	7.1E-11 kmol/m^2/s/kPa
ID	1.0E-4 m
Z	0.50 m
T	300 K
μ	1.7E-5 Pa·s

CONCLUSIONS

We evaluated the performance of five novel ISP designs. Three are based on the use of a hollow fiber fabric or alternating fiber sheets. Two module design parameters, A_r and γ_{IH}, were chosen to maximize permeate recovery for a given purity. These parameters can have a significant impact on performance. For example, the recovery of a fixed purity permeate can change by an order of magnitude with changes in γ_{IH}.

All of the ISP designs can produce permeates of higher purities than that achievable in a conventional countercurrent design. The interest in ISP designs arises from this remarkable behavior.

The increase in recovery afforded by ISP designs comes at the cost of increased area requirements. The area requirement can be more than an order of magnitude larger than that for a countercurrent design. The impact of ISP designs will be limited by this constraint. ISP designs will be competitive only for high purity applications where membrane costs are much smaller than compression costs.

The co-counter design gives the highest permeate recovery of all the designs considered. The next best performer, the co-cross design, is one of the new designs.

Those designs in which the intermediate-pressure permeate and the retentate are contacted co-currently outperform those designs with either cross or countercurrent contacting. The contacting pattern for the low-pressure and intermediate-pressure permeate has less of an impact on performance but those designs with countercurrent contacting of the low-pressure permeate and retentate give the best performance.

In practice, a manufacturer would produce a small number of different mod-

ules with discrete A_r values. To evaluate the impact of not using the optimal value of A_r, the performance of the co-counter design was evaluated for a fixed value of $A_r = 1.5$. This value lies in the middle of the range of values that gave optimal performance. Fixing A_r led to virtually no change in permeate recovery, and the required dimensionless area increased slightly at the higher purities. The results suggest that fixing A_r will have a small effect on performance.

We believe the most promising applications for ISP technology are hydrogen recovery from refinery and petrochemical process streams. In such applications, hydrogen is separated from methane. The process must produce a high purity hydrogen stream (commonly in excess of 90%) at high recoveries (hydrogen recoveries over 90%). The literature describes staged module processes to recover hydrogen in which the extra area required by staging is offset by savings in recompression costs (1). ISP technology offers unique staging opportunities for these applications. Additionally, we believe membrane area costs will decrease as the technology matures. Consequently, applications such as the production of an enriched oxygen stream from air may become economically attractive in the future.

The objectives of this work were to present five new ISP designs and provide detailed performance evaluations that could be used to guide new separation process development. Determination of the economically optimum process will require comparison of single conventional stages, single ISP stages, and cascades of both. Such an optimization is beyond the scope of this work, but the results should help manufacturers optimize configurations by identifying the most promising ISP designs to include in the optimization process.

ACKNOWLEDGMENT

The authors gratefully acknowledge partial support of this project by the National Science Foundation through Grant CTS-9408414.

SYMBOLS

A	permeation area (m^2)
A_r	ratio of area available for intermediate-to-low pressure permeation to area available for high-to-intermediate pressure permeation
F	feed molar flow rate ($mol \cdot s^{-1}$)
ID	fiber inner diameter (m)
J	dimensionless molar permeation rate
l	effective membrane diffusion distance (m)
N_h	dimensionless group defined by Eq. (2)
N_p	dimensionless group defined by Eq. (15)
P	permeability ($mol \cdot m \cdot Pa^{-1} \cdot m^{-2} \cdot s^{-1}$)

p	pressure (Pa)
R	ideal gas constant ($Pa \cdot m^3 \cdot mol^{-1} \cdot K^{-1}$)
T	temperature (K)
x	mole fraction of faster permeating component in retentate
x_f	mole fraction of faster permeating component in feed
y	mole fraction of faster permeating component in permeate
z	dimensionless flow path length
Z	active module length (m)
μ	viscosity (Pa·s)
α	separation factor or permselectivity
γ	pressure ratio
θ	dimensionless molar flow rate
Π	dimensionless pressure

Subscripts and Superscripts

A	faster permeating component
B	slower permeating component
F	feed
H	retentate
HI	from retentate to intermediate-pressure permeate
I	intermediate-pressure permeate
IH	ratio of value for intermediate-pressure permeate to value for retentate
IL	from intermediate-pressure permeate to low-pressure permeate
L	low-pressure permeate
LH	ratio of value for low-pressure permeate to value for retentate
LI	ratio of value for low-pressure permeate to value for intermediate-pressure permeate

REFERENCES

1. R. R. Zolandz and G. K. Fleming, "Gas Permeation," in *Membrane Handbook* (W. S. Ho and K. K. Sirkar, Eds.), Van Nostrand Reinhold, New York, NY, 1992, pp. 17–95.
2. S.-T. Hwang and K. Kammermeyer, *Membranes in Separations*, Wiley-Interscience, New York, NY, 1975.
3. G. G. Lipscomb "Design of Hollow Fiber Contactors for Membrane Gas Separations," in *The 1996 Membrane Technology Review*, Business Communications Co., Norwalk, CT, 1996, pp. 23–102.
4. S. Weller and W. A. Steiner, "Separation of Gases by Fractional Permeation through Membranes," *J. Appl. Phys.*, *23*, 279–283 (1950).
5. S. Weller and W. A. Steiner, "Engineering Aspects of Separation of Gases," *Chem. Eng. Prog.*, *46*, 585–590 (1950).
6. S. A. Stern and W. P. Walawender, "Analysis of Membrane Separation Parameters," *Sep. Sci.*, *4*, 129–159 (1969).
7. W. P. Walawender and S. A. Stern, "Analysis of Membrane Separation Parameters. II.

MARCEL DEKKER, INC.
270 Madison Avenue, New York, New York 10016

Counter-current and Co-current Flow in a Single Permeation Stage, *Ibid*., *7*, 553–584 (1972).
8. C. T. Blaisdell and K. Kammermeyer, "Counter-current and Co-current Gas Separation," *Chem. Eng. Sci*., *28*, 1249–1255 (1973).
9. C. R. Antonson, R. J. Gardner, C. F. King, and D. Y. Ko. "Analysis of Gas Separations by Permeation in Hollow Fibers," *Ind. Eng. Chem., Process Des. Dev*., *16*, 463–469 (1977).
10. Y. Shindo, T. Hakutta, H. Yoshitome, and H. Inoue, "Calculation Methods for Multicomponent Gas Separation by Permeation," *Sep. Sci. Technol*., *20*, 445–459 (1985).
11. F. P. McCandless, "Iterative Solution of Multicomponent Permeator Model Equations," *J. Membr. Sci*., *48*, 115–122 (1990).
12. K. Li, D. R. Acharya, and R. Hughes, "Mathematical Modeling of Multicomponent Membrane Permeators," *Ibid*., *52*, 205–219 (1990).
13. D. T. Coker, B. D. Freeman, and G. K. Fleming, "Modeling Multicomponent Gas Separation Using Hollow-Fiber Membrane Contactors," *AIChE J*., *44*, 1289–1302 (1998).
14. F. P. McCandless, "A Comparison of Some Recycle Permeators for Gas Separation," *J. Membr. Sci*., *24*, 15–28 (1985).
15. S. Majumdar, L. B. Heit, A. Sengupta, and K. K. Sirkar, "An Experimental Investigation of Oxygen Enrichment in a Silicone Capillary Permeator with Permeate Recycle," *Ind. Eng. Chem. Res*., *26*, 1434–1441 (1987).
16. R. W. Naylor and P. O. Backer, "Enrichment Calculations in Gaseous Diffusion: Large Separation Factor," *AIChE J*., *1*, 95–99 (1955).
17. S.-T. Hwang and K. Kammermeyer, "Operating Lines in Cascade Separation of Binary Mixtures," *Can J. Chem. Eng*., *43*, 36–39 (1965).
18. C. Y. Pan and H. W. Habgood, "Gas Separation by Permeation. Part I: Calculation Methods and Parametric Analysis," *Ibid*., *56*, 197–209 (1978).
19. W. C. Pfefferle, "Diffusion Purification of Gases," US Patent 3,144,313 (1964).
20. S.-T. Hwang and J. M. Thorman, "The Continuous Membrane Column," *AIChE J*., *26*, 558–566 (1980).
21. M. Sekino, K. Chikanari, and T. Taniyama, "Hollow Fiber Membrane Separations Apparatus, US Patent 4,293,419 (1981).
22. D. W. Edwards, "Multiple Bundle Fluid Separation Apparatus," US Patent 4,670,145 (1987).
23. M. J. Coplan "Module for Multistage Gas Separation, US Patent 4,676,808 (1987).
24. P. S. Puri and D. G. Kalthod, "Multiple Stage Countercurrent Hollow Fiber Membrane Module," US Patent 5,176,725 (1993).
25. S. Kimira, T. Nomura, T. Miyauchi, and M. Ohno, "Separation of Rare Gases by Membranes," *Radiochem. Radioanal. Lett*., *13*, 349–354 (1973).
26. M. Sidhoum, S. Majumdar, R. R. Bhave, and K. K. Sirkar, "Experimental Behavior of Asymmetric CA Membranes and Its Use in Novel Separation Schemes," *AIChE Symp. Ser*., *84*, 102–112 (1988).
27. K. Li, D. R. Acharya, and R. Hughes, "Simulation of Gas Separation in an Internally Staged Permeator," *Trans. Inst. Chem. Eng*., *69*, 35–42 (1991).
28. K. Li, D. R. Acharya, and R. Hughes, "Gas Separation in an Internally Staged Permeator: Experimental Results and Theoretical Predictions, *J. Membr. Sci*., *80*, 147–156 (1993).
29. Y. S. Chen, K. Li, and W. K. Teo, "Performance of Co/Counter-Current and Counter/Co-Current Flow Patterns in an Internally Staged Permeator for Gas Separation," *Chem. Eng. Res. Des*., *73*, 567–574 (1995).
30. K. Li and R. Hughes, "Internally Staging for Membrane Gas Separation: Comparison with Conventional Membrane Permeators," *Chem. Eng. Sci*., *48*, 3795–3803 (1993).
31. K. Li, D. Wang, D. Li, and W. K. Teo, "Internally Staged Permeator Prepared from An-

MARCEL DEKKER, INC.
270 Madison Avenue, New York, New York 10016

nular Hollow Fibers for Gas Separation," *AIChE J.*, *44*, 849–858 (1998).
32. K. Li, W. W. Y. Lau, and W. K. Teo, "Theoretical and Experimental Evaluation of an Internally Multi-Staged Permeator for Oxygen Enrichment," *Chem. Eng. Sci.*, *49*, 2405–2412 (1994).
33. W. J. Koros and R. T. Chern, in *Handbook of Separation Process Technology* (R. W. Rousseau, Ed.), Wiley, New York, NY, 1987.
34. MATLAB™, The MathWorks Inc., Natick, MA.
35. W. H. Press, B. P. Flannery, S. A. Teukolsky, and W. T. Vetterling, *Numerical Recipes in Pascal*, Cambridge University Press, New York, NY, 1989.

Received by editor July 12, 1999
Revision received October 1999

Request Permission or Order Reprints Instantly!